P H Y S I C A L   R E V I E W   L E T T E R S

Search for Light Dark Matter in XENON10 Data

J. Angle,[1,2] E. Aprile,[3] F. Arneodo,[4] L. Baudis,[2] A. Bernstein,[5] A. I. Bolozdynya,[6] L. C. C. Coelho,[7] C. E. Dahl,[8]
L. DeViveiros,[9] A. D. Ferella,[2,4] L. M. P. Fernandes,[7] S. Fiorucci,[9] R. J. Gaitskell,[9] K. L. Giboni,[3] R. Gomez,[10] R. Hasty,[11]
L. Kastens,[11] J. Kwong,[8] J. A. M. Lopes,[7] N. Madden,[5] A. Manalaysay,[1,2] A. Manzur,[11] D. N. McKinsey,[11]
M. E. Monzani,[3] K. Ni,[11] U. Oberlack,[10,12] J. Orboeck,[13] G. Plante,[3] R. Santorelli,[3] J. M. F. dos Santos,[7] S. Schulte,[13]
P. Shagin,[10] T. Shutt,[6] P. Sorensen,[5,*] C. Winant,[5] and M. Yamashita[3]

(XENON10 Collaboration)

[1]*Department of Physics, University of Florida, Gainesville, Florida 32611, USA*
[2]*Physics Institute, University of Zürich, Winterthurerstrasse 190, CH-8057, Zürich, Switzerland*
[3]*Department of Physics, Columbia University, New York, New York 10027, USA*
[4]*Gran Sasso National Laboratory, Assergi, L'Aquila, 67010, Italy*
[5]*Lawrence Livermore National Laboratory, 7000 East Avenue, Livermore, California 94550, USA*
[6]*Department of Physics, Case Western Reserve University, Cleveland, Ohio 44106, USA*
[7]*Department of Physics, University of Coimbra, R. Larga, 3004-516, Coimbra, Portugal*
[8]*Department of Physics, Princeton University, Princeton, New Jersey 08540, USA*
[9]*Department of Physics, Brown University, Providence, Rhode Island 02912, USA*
[10]*Department of Physics and Astronomy, Rice University, Houston, Texas 77251, USA*
[11]*Department of Physics, Yale University, New Haven, Connecticut 06511, USA*
[12]*Johannes Gutenberg University Mainz, 55099 Mainz, Germany*
[13]*Department of Physics, RWTH Aachen University, Aachen, 52074, Germany*
(Received 14 April 2011; revised manuscript received 3 June 2011; published 27 July 2011)

We report results of a search for light ($\lesssim 10$ GeV) particle dark matter with the XENON10 detector. The event trigger was sensitive to a single electron, with the analysis threshold of 5 electrons corresponding to 1.4 keV nuclear recoil energy. Considering spin-independent dark matter-nucleon scattering, we exclude cross sections $\sigma_n > 7 \times 10^{-42}$ cm^2, for a dark matter particle mass $m_\chi = 7$ GeV. We find that our data strongly constrain recent elastic dark matter interpretations of excess low-energy events observed by CoGeNT and CRESST-II, as well as the DAMA annual modulation signal.

Recently, the CRESST-II and CoGeNT collaborations have reported the observation of low-energy events in excess of known backgrounds [1,2]. This has encouraged the hypothesis that these signals—in addition to the long-standing DAMA [3] annual modulation signal—might arise from the scattering of a light ($\lesssim 10$ GeV) dark matter particle [4–10]. The CDMS [11,12] dark matter search data been have reanalyzed with lowered energy thresholds, but do not fully exclude light dark matter interpretations. In order to maintain sensitivity to the scattering of such light galactic dark matter, an experiment needs either a very low $\mathcal{O}$(keV) energy threshold, as with CoGeNT, or light target nuclei, such as the oxygen atoms in the CRESST-II detector. This is a simple requirement of the kinematics [13]. For example, consider a halo-bound dark matter particle with mass $m_\chi = 10$ GeV and velocity 600 km s^{-1}. The maximum recoil energy that would result from an elastic scatter of such a particle in an earth-bound target would be about 20 keV for a recoiling oxygen nucleus (CRESST-II), 9 keV for germanium (CoGeNT) and only 6 keV for xenon. The respective energy thresholds of CRESST-II and CoGeNT are approximately 10 keV [14] and 2 keV [2], which

combined with a low background event rate results in good sensitivity to light mass dark matter. The energy threshold of previously reported XENON10 data [15,16] depended on the primary scintillation efficiency of liquid xenon for nuclear recoils ($\mathcal{L}_{\text{eff}}$) [17,18]. For a conservative assumption of the energy dependence of $\mathcal{L}_{\text{eff}}$ [17], the threshold was about 5 keV.

It is possible to obtain a lower-energy threshold from existing XENON10 dark matter search data, if nuclear recoil energy is measured by the detected electron signal. The method allows us to reach an energy threshold $E_{\text{nr}} \sim 1$ keV. At such low nuclear recoil energies, the primary scintillation signal is generally absent. As a result, two important aspects of the XENON10 detector [19] performance are compromised: the ability to precisely reconstruct the z coordinate of a particle interaction, and the discrimination between incident particle types. The detected ratio of scintillation to electron signals was used in [15,16] to discriminate and reject about 99.5% of electromagnetic background events which would otherwise have been treated as dark matter candidate events. Loss of this discrimination thus reduces our sensitivity to

nuclear recoils from dark matter scattering, by about 2
orders of magnitude. Still, the lower-energy threshold we
obtain permits the exploration of new regions of dark
matter particle mass (m_χ) and cross section (σ_n) parameter
space.

The XENON10 detector is described in detail in [19].
For the present discussion, we remind the reader that
XENON10 observes particle interactions via detected pri-
mary scintillation photons (the $S1$ signal) and electrons
(the $S2$ signal). The electrons are drifted across the liquid
xenon target and extracted into gaseous xenon, where they
create proportional scintillation photons. This allows both
$S1$ and $S2$ to be observed with the same photomultiplier
tube arrays. A single electron extracted from the liquid
target results in about 27 photoelectrons in the photomul-
tiplier arrays. It is this robust signal that gives the $S2$
channel its lower-energy threshold. The (x, y) coordinates
of particle interactions are reconstructed from the hit pat-
tern of the $S2$ signal on the top photomultipliers. The z
coordinate is usually reconstructed from $z = v_d \Delta t$, where
$v_d \simeq 0.20$ cm μs^{-1} is the electron drift velocity [20] and
Δt is the measured time delay between the $S1$ and $S2$. This
method cannot be used if there is no $S1$ signal, as is often
the case for very low-energy nuclear recoils [21]. The $S2$
pulse width σ_e carries a mild z dependence [22]. Larger
detectors [23,24], if operated with a lower value of E_d, may
obtain a reliable estimate of the z coordinate from σ_e [25];
this should lead to a significant rejection of edge (in z)
events and a commensurate improvement in sensitivity.

Ideally we would like to reconstruct the nuclear recoil
energy for each event from $E_{\mathrm{nr}} = \epsilon(n_\gamma + n_e)/f_n$, as in
[26,27], with $\epsilon = 13.8$ eV the average energy to create a
photon or electron, and f_n the nuclear recoil quenching
[28]. However, at low recoil energies the small number n_γ
of primary scintillation photons often does not result in a
measurable $S1$ response. Since we are interested in events
at very low recoil energy, we calibrate the energy scale
using only the number n_e of measured electrons in the $S2$
signal. The electron yield of liquid xenon for nuclear
recoils has been measured directly using tagged neutron
scattering [17,29]. The lowest-energy data point from [17]
implies an $S2$ signal of 36 ± 6 electrons in the 3–5 keV
range, as shown in Fig. 1. An indirect measurement of the
electron yield is described in [22], and was obtained fol-
lowing the method detailed in [21]. The central and $\pm 1\sigma$
contours of that work are shown in Fig. 1 (dash-dot curves).
That Q_y rises with decreasing E_{nr} between 100 and 10 keV
is a result of the increasing fraction of nuclear recoil energy
given to electrons (rather than photons) over that energy
range [26].

Following [26], we obtain a theoretical prediction for the
electron yield,

$$Q_y \equiv \frac{n_e}{E_{\mathrm{nr}}} = \frac{1}{\xi} \ln(1 + \xi) \frac{f_n(k)/\epsilon}{1 + N_{\mathrm{ex}}/N_i}. \tag{1}$$
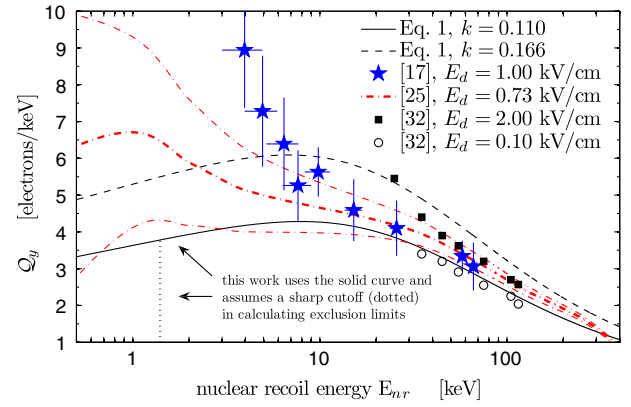

FIG. 1 (color online). The electron yield Q_y of liquid xenon
for nuclear recoils. Theoretical curves (solid and dashed) were
calculated from Eq. (1), as described in the text. Also shown are
measurements from [17] (★), [22] (dash-dot curve, with $\pm 1\sigma$
contours), and [29] ($\bigcirc$ and $\blacksquare$, uncertainty omitted for clarity).

In this equation, N_{ex}/N_i is the number ratio of excited to
ionized xenon atoms, and $\xi = N_i \alpha/(4a^2 v)$ is the single
parameter upon which the Thomas-Imel box model de-
pends [30,31]. In Eq. (1) we explicitly indicate the depen-
dence of f_n on the proportionality constant k, between the
velocity of a xenon nucleus and its electronic stopping
power. In Fig. 1 we show Eq. (1) predictions for two k
values, which correspond to calculations by Lindhard [28]
and Hitachi [29]. The dashed curve is the best-fit case from
[26], with $k = 0.166$, $N_{\mathrm{ex}}/N_i = 1.05$ and $4\xi/N_i = 0.024$.
The solid curve, which we will use to calibrate the energy
scale in the present work, takes the more conservative
$k = 0.110$, from which we obtain the best-fit parameters
$N_{\mathrm{ex}}/N_i = 1.09$ and $4\xi/N_i = 0.032$. This results in the
most conservative σ_n exclusion limits based on available
data and theoretical considerations, and is consistent
with our neutron calibration data [22]. However, it
is in tension with the measurements of Ref. [17] below
~7 keV. As discussed in [32], the rising measured Q_y
values in this regime could be influenced by trigger thresh-
old bias. We emphasize that our energy calibration
(Fig. 1, solid curve) relies on extrapolation of Lindhard's
theory [28] below 4 keV.

We report results from a 12.5 live day dark matter
search, obtained between August 23 and September 14,
2006. This data set is distinct from the previously reported
[15,16] XENON10 dark matter search data: the present
data was obtained with the the secondary scintillation gain
about 12% higher, and the $S2$-sensitive trigger threshold
set at the level of a single electron. The trigger efficiency
for single electrons is >0.80 [33].

Event selection criteria are summarized in Table I.
Candidate events were required to have an $S2$ signal of at
least 5 electrons, or 1.4 keV. Although the detector is
sensitive to smaller energy depositions, we are unable to
reliably assess the cut acceptance ε_c for smaller nuclear
recoils, due to the trigger configuration during the neutron

TABLE I. Summary of cuts applied to 15 kg days of dark matter search data, corresponding acceptance for nuclear recoils ε_c and number of events remaining in the range $1.4 < E_{nr} \leq 10$ keV.

	Cut description	ε_c	N_{evts}
1.	event localization $r < 3$ cm	1.00[a]	125
2.	signal-to-noise	>0.94	58
3.	single scatter (single $S2$)	>0.99	38
4.	$\pm 3\sigma$ nuclear recoil band	>0.99	23

[a]Limits effective target mass to 1.2 kg.

calibration [19]. The position of interaction was required to fall within $r < 3$ cm. This central region features optimal self-shielding by the surrounding xenon target. A signal-to-noise cut required the $S2$ pulse to contain at least 0.45 of the total area of the event record. The acceptance of this cut rises monotonically from 0.94 to >0.99 between 1.4 keV and 10 keV. Valid single scatter event records were required to have only a single $S2$ pulse of size >4 electrons. Events in which an $S1$ signal was found were required to have $\log_{10}(S2/S1)$ within the $\pm 3\sigma$ band for elastic single scatter nuclear recoils. This band was determined from the neutron calibration data, and has been reported in a previous article [15]. Events in which no $S1$ signal was found were assumed to be dark matter candidate events and were retained.

The remaining events in the lowest-energy region are shown in Fig. 2 (left) versus their $S2$ pulse width σ_e. The equivalent number of electrons is indicated by the inset scale. Events in which an $S1$ signal was observed are
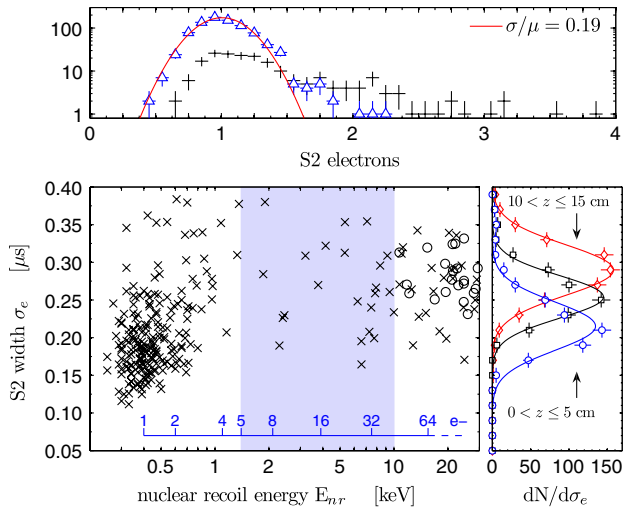

FIG. 2 (color online). (left) All candidate dark matter events remaining ($\times$ and $\bigcirc$) after the cuts listed in Table I. Events in which an $S1$ was found are shown as $\bigcirc$. The number of electrons in the $S2$ signal is indicated by the inset scale. (top) Distribution of candidate events with ≤ 4 electrons (+), and distribution of background single electrons ($\triangle$) as described in the text. (right) $S2$ pulse width distributions for single scatter nuclear recoils in the top, middle and bottom third of the detector.

indicated by a circle. Figure 2 (right) shows the width profile of the $S2$ signal in the top, middle and bottom third of the detector, based on single scatter nuclear recoils with known Δt and $5 < S2 < 100$ electrons. Gaussian fits are shown to guide the eye.

The top panel of Fig. 2 shows the distribution of remaining candidate events (+) with $S2 \leq 4$ electrons. The distribution of background single electron events, sampled from a time window at least 20 μs after higher-energy events, is also shown ($\triangle$). The single electron background events are a subject of ongoing study, and appear to originate from multiple physical phenomena. One possibility involves photoionization of impurities in the liquid xenon [34]. Another possible origin is from excess free electrons trapped at the liquid surface. This could occur because the emission of electrons from the liquid to the gas is nearly— but likely not exactly—unity [35]. As a result, every $S2$ signal could be a potential source of a small number of trapped electrons. Delayed emission of the trapped electrons may result from the requirement that both the electron kinetic energy and the z component of the electron momentum be sufficient to overcome the surface potential barrier [36].

The signal-to-noise cut was motivated by a distinct but closely related class of background event, which consists of a train of approximately ten to several tens of single electrons over a period of $\mathcal{O}(100 \, \mu$s). The origin of these events is also not yet clear. Often several single electrons in an electron train overlap in time, to the degree that they appear as a single $S2$ pulse containing $\sim$2–6 electrons. These spurious pulses often have $\sigma_e > 0.30$ (the 3σ width for a single electron) and so could be removed based on pulse width. However, the signal-to-noise cut more precisely targets the presence of multiple additional single electrons in the event record.

The energy resolution for $S2$ signals depends primarily on Poisson fluctuation in the number of detected electrons, with an additional component due to instrumental fluctuations. This is discussed in detail in [32], and for higher-energy signals in [19]. So as not to overstate the energy resolution, we adopt a parameterization which follows the Poisson component only, given by $\mathcal{R}(E_{nr}) = (2E_{nr})^{-1/2}$. We assume a sharp cutoff in $\mathcal{Q}_y$ at $E_{nr} = 1.4$ keV, and then convolve the resolution with the predicted differential dark matter scattering rate. This ensures that σ_n exclusion limits are not influenced by lower-energy extrapolation of the detector response. The scattering rate as a function of nuclear recoil energy was calculated in the usual manner [13] (cf. [15]). We take the rotational speed of the local standard of rest and the velocity dispersion of the dark matter halo to be $v_0 = 230$ km s^{-1}, and the galactic escape velocity to be $v_{esc} = 600$ km s^{-1} [37]. We use the p_{max} method [38] to calculate 90% C.L. exclusion limits on the cross section σ_n for elastic spin-independent dark matter—nucleon scattering as a function of m_χ. All remaining
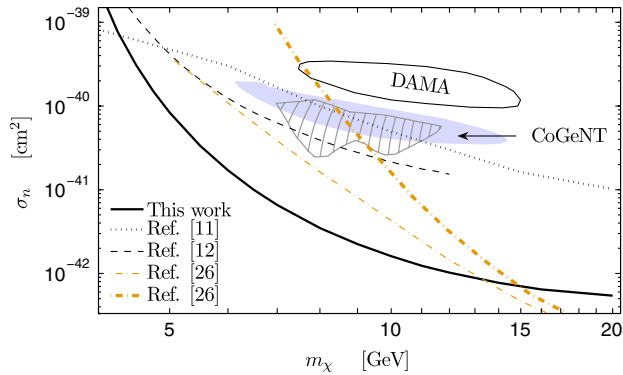
FIG. 3 (color online). Curves indicate 90% C.L. exclusion limits on spin-independent σ_n for elastic dark matter scattering, obtained by CDMS (dotted [11], and dashed [12]) and XENON100 (dash-dot [23]). The region consistent with assumption of a positive detection by CoGeNT is shown (hatched) [2], and (shaded) [4]; the latter assumes a 30% exponential background. Also shown is the 3σ allowed region for the DAMA annual modulation signal (solid contour) [43].

events in the the range $E_{nr} > 1.4$ keV are treated as potential dark matter signal. The results are shown in Fig. 3. If Q_y were 40% higher (lower) below 4 keV, the exclusion limits would be about $\times 2$ stronger (weaker) at $m_\chi = 7$ GeV.

The exclusion limits and allowed regions shown in Fig. 3 assume a simple Maxwell-Boltzman distribution for the dark matter halo. Given the likelihood of significant departures from this distribution [39], it is important to understand if astrophysical uncertainties could alter the incompatibility of our results with the positive detection scenarios shown in Fig. 3. A method for doing so is described in [40], and predicts that not less than ~ 5 counts keV^{-1} kg^{-1} day^{-1} should be observed in a xenon detector, if the unexplained low-energy rise observed by the CoGeNT detector [2] were due to dark matter scattering. It can be seen from Table I that we observe an event rate of ~ 0.2 counts keV^{-1} kg^{-1} day^{-1} on the interval $1.4 < E_{nr} < 10$ keV, indicating that the order of magnitude exclusion of the CoGeNT regions shown in Fig. 3 is robust against astrophysical uncertainties. Because of the preliminary nature of the CRESST-II results we do not show a corresponding allowed region, although it appears likely to lie above the DAMA region, as shown in Fig. 3 of Ref. [41].

We have shown for the first time that it is possible to perform a sensitive search for dark matter with a liquid xenon time-projection chamber, using only the electron signal. The advantage of this analysis is an increased sensitivity to light ($\lesssim 10$ GeV) dark matter candidate particles, due to the approximate factor $\times 5$ decrease in the detector energy threshold. For larger particle masses, standard analyses [15,23,42] offer superior sensitivity. The present work appears to severely constrain recent light elastic dark matter interpretations of the excess low-energy events observed by CoGeNT and CRESST-II, as well as interpretations of the DAMA modulation signal.

*pfs@llnl.gov

[1] W. Seidel (CRESST-II Collaboration) at *IDM2010 Conference, Univ. of Montpellier 2, Montpellier FR, July 26–30*, 2010.

[2] C. E. Aalseth *et al.* (CoGeNT Collaboration), Phys. Rev. Lett. **106**, 131301 (2011).

[3] R. Bernabei *et al.* (DAMA/LIBRA), Eur. Phys. J. C **56**, 333 (2008).

[4] S. Chang, J. Liu, A. Pierce, N. Weiner, and I. Yavin, J. Cosmol. Astropart. Phys. 08 (2010) 018.

[5] P. W. Graham, R. Harnik, S. Rajendran, and P. Saraswat, Phys. Rev. D **82**, 063512 (2010).

[6] R. Essig, J. Kaplan, P. Schuster, and N. Toro, arXiv:1004.0691.

[7] D. Hooper, J. I. Collar, J. Hall, D. N. McKinsey, and C. M. Kelso, Phys. Rev. D **82**, 123509 (2010).

[8] A. L. Fitzpatrick and K. M. Zurek, Phys. Rev. D **82**, 075004 (2010).

[9] B. Feldstein, P. W. Graham, and S. Rajendran, Phys. Rev. D **82**, 075019 (2010).

[10] A. Bottino, F. Donato, N. Fornengo, and S. Scopel, Phys. Rev. D **81**, 107302 (2010).

[11] D. S. Akerib *et al.* (CDMS Collaboration), Phys. Rev. D **82**, 122004 (2010).

[12] Z. Ahmed *et al.* (CDMS Collaboration), Phys. Rev. Lett. **106**, 131302 (2011).

[13] J. D. Lewin and P. F. Smith, Astropart. Phys. **6**, 87 (1996).

[14] G. Angloher *et al.*, Astropart. Phys. **31**, 270 (2009).

[15] J. Angle *et al.* (XENON10 Collaboration), Phys. Rev. D **80**, 115005 (2009).

[16] J. Angle *et al.* (XENON10 Collaboration), Phys. Rev. Lett. **100**, 021303 (2008).

[17] A. Manzur *et al.*, Phys. Rev. C **81**, 025808 (2010).

[18] E. Aprile *et al.*, Phys. Rev. C **79**, 045807 (2009).

[19] E. Aprile *et al.* (XENON10 Collaboration), Astropart. Phys. **34**, 679 (2011).

[20] E. M. Gushchin, A. A. Kruglov, and I. M. Obodovskii, Sov. Phys. JETP **55**, 650 (1982).

[21] P. Sorensen *et al.* (XENON10 Collaboration), Nucl. Instrum. Methods Phys. Res., Sect. A **601**, 339 (2009).

[22] P. Sorensen *et al.* (XENON10 Collaboration), Proc. Sci., IDM2010 (2010) 017 [arXiv:1011.6439].

[23] E. Aprile *et al.* (XENON100 Collaboration), Phys. Rev. Lett. **105**, 131302 (2010).

[24] D. N. McKinsey *et al.* (LUX), J. Phys. Conf. Ser. **203**, 012026 (2010).

[25] P. Sorensen, Nucl. Instrum. Methods Phys. Res., Sect. A **635**, 41 (2011).

[26] P. Sorensen and C. E. Dahl, Phys. Rev. D **83**, 063501 (2011).

[27] T. Shutt *et al.*, Nucl. Instrum. Methods Phys. Res., Sect. A **579**, 451 (2007).

[28] J. Lindhard, V Nielsen, M. Scharff, and P. V. Thomsen, K. Dan. Vidensk. Selsk. Mat. Fys. Medd. **33**, 10 (1963).

[29] E. Aprile *et al.*, Phys. Rev. Lett. **97**, 081302 (2006).

[30] J. Thomas and D. A. Imel, Phys. Rev. A **36**, 614 (1987).

[31] The model describes N_i initial electron-ion pairs in a box of dimension a, with recombination coefficient α and average electron drift velocity v.

[32] P. Sorensen, J. Cosmol. Astropart. Phys. 09 (2010) 033.

[33] P. Sorensen, Ph.D. thesis, Brown University, 2008, Providence, RI.

[34] B. Edwards *et al.* (ZEPLIN-II Collaboration), Astropart. Phys. **30**, 54 (2008).

[35] E. M. Gushchin, A. A. Kruglov, and I. M. Obodovskii, Sov. Phys. JETP **55**, 860 (1982).

[36] A. I. Bolozdynya, Nucl. Instrum. Methods Phys. Res., Sect. A **422**, 314 (1999).

[37] M. C. Smith *et al.*, Mon. Not. R. Astron. Soc. **379**, 755Ð772 (2007).

[38] S. Yellin, Phys. Rev. D **66**, 032005 (2002).

[39] M. Kuhlen *et al.*, J. Cosmol. Astropart. Phys. 02 (2010) 030.

[40] P. J. Fox, J. Liu, and N. Weiner, Phys. Rev. D **83**, 103514 (2011).

[41] T. Schwetz, arXiv:1011.5432.

[42] E. Aprile *et al.* (XENON100 Collaboration), arXiv:1104.2549.

[43] C. Savage, G. Gelmini, P. Gondolo, and K. Freese, Phys. Rev. D **83**, 055002 (2011).